APL Materials

RESEARCH ARTICLE | DECEMBER 16 2022

On the thermal and mechanical properties of $Mg_{0.2}Co_{0.2}Ni_{0.2}Cu_{0.2}Zn_{0.2}O$ across the high-entropy to entropy-stabilized transition

Special Collection: Design and Development of High Entropy Materials

Christina M. Rost ; Daniel L. Schmuckler ; Clifton Bumgardner ; Md Shafkat Bin Hoque; David R. Diercks ; John T. Gaskins ; Jon-Paul Maria; Geoffrey L. Brennecka ; Xiadong Li ; Patrick E. Hopkins

APL Mater. 10, 121108 (2022)
https://doi.org/10.1063/5.0122775

On the thermal and mechanical properties of $Mg_{0.2}Co_{0.2}Ni_{0.2}Cu_{0.2}Zn_{0.2}O$ across the high-entropy to entropy-stabilized transition

Cite as: APL Mater. 10, 121108 (2022); doi: 10.1063/5.0122775
Submitted: 25 August 2022 • Accepted: 23 November 2022 •
Published Online: 16 December 2022

Christina M. Rost,[1,a)] Daniel L. Schmuckler,[1] Clifton Bumgardner,[2] Md Shafkat Bin Hoque,[2] David R. Diercks,[3] John T. Gaskins,[4] Jon-Paul Maria,[5] Geoffrey L. Brennecka,[3] Xiadong Li,[2] and Patrick E. Hopkins[6,7,2]

AFFILIATIONS

[1] Department of Physics and Astronomy, James Madison University, Harrisonburg, Virginia 22807, USA
[2] Department of Mechanical and Aerospace Engineering, University of Virginia, Charlottesville, Virginia 22904, USA
[3] Department of Metallurgical and Materials Engineering, Colorado School of Mines, Golden, Colorado 80401, USA
[4] Laser Thermal, Charlottesville, Virginia 22902, USA
[5] Department of Materials Science and Engineering, The Pennsylvania State University, University Park, Pennsylvania 16802, USA
[6] Department of Materials Science and Engineering, University of Virginia, Charlottesville, Virginia 22904, USA
[7] Department of Physics, University of Virginia, Charlottesville, Virginia 22904, USA

Note: This paper is part of the Special Topic on Design and Development of High Entropy Materials.
[a)] **Author to whom correspondence should be addressed:** rostcm@jmu.edu

ABSTRACT

As various property studies continue to emerge on high entropy and entropy-stabilized ceramics, we seek a further understanding of the property changes across the phase boundary between "high-entropy" and "entropy-stabilized" phases. The thermal and mechanical properties of bulk ceramic entropy stabilized oxide composition $Mg_{0.2}Co_{0.2}Ni_{0.2}Cu_{0.2}Zn_{0.2}O$ are investigated across this critical transition temperature via the transient plane-source method, temperature-dependent x-ray diffraction, and nano-indentation. The thermal conductivity remains constant within uncertainty across the multi-to-single phase transition at a value of ≈2.5 W/mK, while the linear coefficient of thermal expansion increases nearly 24% from 10.8 to 14.1×10^{-6} K^{-1}. Mechanical softening is also observed across the transition.

I. INTRODUCTION

The surge of scientific interest surrounding novel, multidimensional material compositions such as medium and high entropy alloys (MEAs and HEAs),[1–4] multicomponent alloys,[5] multi-principal element alloys (MPEAs), complex concentrated alloys (CCAs), and their analogous ceramic-based compositions[6–8] is building pathways for understanding unique and complex structure–property relationships. Entropy stabilized oxides (ESOs)[6] are one such subclass of high entropy oxides. ESOs add further complexity to the thermodynamic landscape of such materials, particularly those shown to be stabilized through entropic means[9,10]—created through mixing equimolar amounts of several binary oxide components to overcome a positive enthalpy of mixing. The nature of this phase change is physically reversible. Above the critical temperature, the system presents as a single-phase solid solution, which, through quenching, remains metastable at room temperature. If slowly cooled below the critical transition, a multi-phase, high entropy composite is formed, where a secondary phase precipitates from the host matrix. Even with the presence of a secondary phase, the host still exhibits the key characteristic of a high entropy system in that the number of phases present is below predictions from the Gibbs phase rule.[11] Logically, similar to other systems exhibiting structural and/or compositional changes,[12–14] this phase

precipitation and subsequent high-entropy restructuring would be expected to alter material properties.

Property studies continue to emerge on high entropy oxides with an emphasis on functional applications such as catalysis.[15–17] To our knowledge, very little has been done with regard to the property changes through the critical transition temperature. Here, we develop a further understanding of and report on the thermal and mechanical property changes across the phase boundary between "high-entropy" and "entropy-stabilized" phases in bulk ceramic ESO $Mg_{0.2}Co_{0.2}Ni_{0.2}Cu_{0.2}Zn_{0.2}O$.

II. MATERIALS AND METHODS

ESO composition $Mg_{0.2}Co_{0.2}Ni_{0.2}Cu_{0.2}Zn_{0.2}O$ (J14) was synthesized by combining equimolar amounts of MgO, NiO, CoO, CuO, and ZnO binary oxides and mixing/milling using a SPEX SamplePrep (NJ, USA) high-energy ball mill with 5 mm yttria-stabilized zirconia milling media. Mixed powder was pressed into 12 mm diameter pellets by applying 5000 lbs of force using a Carver uniaxial hydraulic press (IN, USA). Green body pellets were reactively sintered at 1273 K for 2 h in an open atmosphere, followed by an air quench. x-ray diffraction (XRD) measurements for phase analysis were performed using a PANalytical Empyrean (Almelo, The Netherlands) diffractometer in Bragg–Brentano geometry with a Chi-Phi-XYZ stage and a PIX'cel detector.

In situ temperature measurements were done at the Analytical Instrumentation Facility (AIF) at North Carolina State University (Raleigh, NC) using an HTK 1200N oven heater stage for the Empyrean. Lattice parameters were determined using the GSAS-II analysis package.[18] A total of 26 x-ray powder diffraction patterns were collected. Each measurement spanned 60° 2θ with a step size of 0.0131°. The sample was heated in 10 K increments at a rate of 10 K/min followed by a 10-min equilibration time before measurement at each temperature. Two regions were measured: 983–1123 K for the multi-phase and 1173–1273 K for the single-phase regimes, respectively. As shown in the temperature heating profile in Fig. S1 in the supplementary material, the sample was first heated through the single-phase transition, measured, then cooled to 973 K, and held for 2 h to ensure phase separation before re-measurement. The Rietveld method[19] was used to find six constants, and then a sequential fit was performed across eight variables. The final R_{wp} values averaged between 2.68 and 4.33. A ten-coefficient Chebyshev background, sample displacement, micro-strain, initial lattice parameters, average cation occupancy, and thermal displacement values were refined at the minimum temperature of each regime. A sequential fit of lattice parameter changes was then performed on each set of diffractograms. For the multi-phase data, refinement of phase fraction was also included. The results can be found in the tables in the supplementary material.

Nanoscale compositional and microstructural analysis through the phase transition was done using transmission electron microscopy (TEM). An FEI Helios Nanolab 600i was used to focus the ion beam mill specimens using a lift-out method. TEM analysis was performed on an FEI Talos F200X instrument operated at 200 keV.

Instrumented indentation, using the Oliver–Pharr methodology,[20,21] was used to extract the high temperature mechanical properties across the phase transition. Indentations were performed

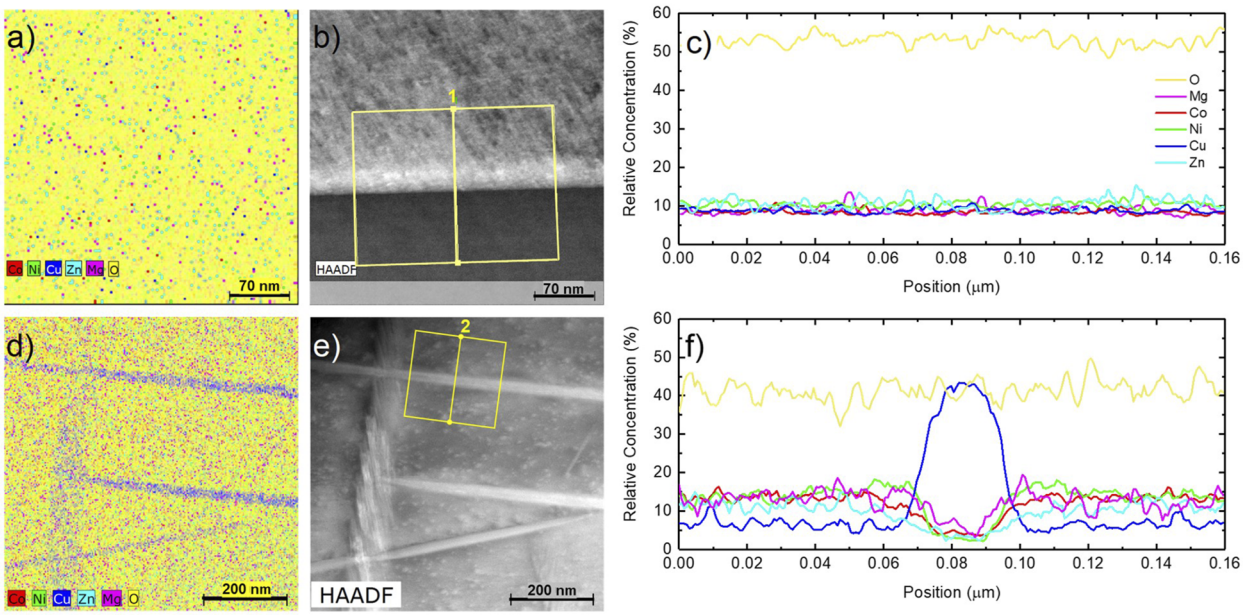

FIG. 1. TEM micrographs and corresponding EDX-measured elemental distributions of both single phase rock salt and phase-separated J14. Panel (a) shows the EDX elemental distribution map, panel (b) is the TEM image associated with the EDX mapping, and panel (c) is an EDX line scan confirming the composition homogeneity across a grain boundary for the single phase, characteristic of the expected rock salt solid solution. Similarly, panels (d)–(f) show the elemental distribution, TEM image, and line scan across the phase boundary, respectively, for the multi-phase regime, where needle-like grains consisting primarily of CuO precipitate from the rock salt host.

at temperatures up to 1223 K on a mechanically polished specimen on a nano-indenter (MicroMaterials NanoTest Vantage) with a cubic boron nitride (cBN) Berkovich indenter tip. A series of ten indentations were performed on the specimen at each temperature as the sample was thermally cycled from the ambient temperature to 1223 K for three cycles within an open-air environment. A consistent heating and cooling rate of 1.6 K/min was used, and the specimen was allowed to stabilize at each temperature for one hour prior to performing the indentation.

The temperature-dependent thermal conductivity of a pair of J14 samples in both single- and multi-phase was measured using the transient plane source system Hot Disk (TPS 3500, Thermtest) from 100 to 600 K. Additional details regarding the hot-disk method can be found elsewhere in the literature.[22,23] Prior to measurements, both samples were annealed in air at 1273 K and 1073 K for 1 h to promote stabilization in the single- and multi-phase, respectively. The Hot Disk TPS 3500 was checked against two reference standards: stainless-steel and a BK7 window glass, and the measured values were found to be in good agreement with the literature.[24–27] The J14 samples were ≈85% dense, estimated via mass/volume calculations, and the thermal conductivity values were subsequently adjusted using the Maxwell Garnett model shown in Eq. (1)[22,28] below, in which ϕ is the relative porosity percentage of the samples,

$$k_{solid} = \frac{k_{porous}}{\frac{1-\phi}{1+\phi}}. \tag{1}$$

III. RESULTS AND DISCUSSION

Figure 1 shows the microstructure and chemical distribution of J14 above and below the transition temperature, characterized via transmission electron microscopy (TEM) and energy dispersive spectroscopy (EDX). Consistent with previous results,[29] the single-phase rock salt solution transitions into a two phase system, where CuO needles precipitate from the rock salt host.

Due to the isotropic nature of the J14 phase, we are able to reduce thermal expansion to one dimension. The linear coefficient of thermal expansion (CTE) for J14 shown in Fig. 2 plots the lattice parameter vs temperature for (a) single phase J14 and (b) Cu deficient J14, as found in the two-phase regime. The slope is used to determine the CTE based on the basic equation

$$\alpha_L = \frac{1}{L}\frac{\Delta L}{\Delta T}, \tag{2}$$

where α_L is the linear CTE, L is the lower limit of the lattice parameter in the measurement, and $\Delta L/\Delta T$ is the slope. Based on these data, we find the CTE for the single phase J14 [Fig. 2(a)] to be $14.12 \pm 0.09 \times 10^{-6}$ K^{-1}. The two-phase temperature regime [Fig. 2(b)] is somewhat more complicated: Cu is actively dissolving back into the rock salt host across the transition back to single phase concurrently with its thermal expansion, creating a superimposed function on the CTE as the host makes room for additional cations. The Rietveld refinement of the weight fractions of CuO and J14 as a function of temperature, shown in Fig. 2(c), suggests a transition range from ~1030 to 1085 K, where the remaining CuO nearly completely dissolves. This temperature range agrees well with the previous observations of the transition from multi-phase to single phase J14.[6] It can be seen that above this transition region, the coefficient of thermal expansion is found to be $14.97 \pm 0.09 \times 10^{-6}$ K^{-1}, an ~4.7% difference from the single phase regime. Referring back to Fig. 2(c), this could be due to 0.6 wt. % Cu still slowly diffusing into the host lattice. Below this transition range, a larger concentration of CuO (≈4 wt. %) exists outside of J14, and the CTE of the primary phase drops to $10.8 \pm 0.3 \times 10^{-6}$ K^{-1}.

Figure 3 shows the thermal conductivity of the single-phase and multi-phase J14 samples as a function of temperature. These thermal

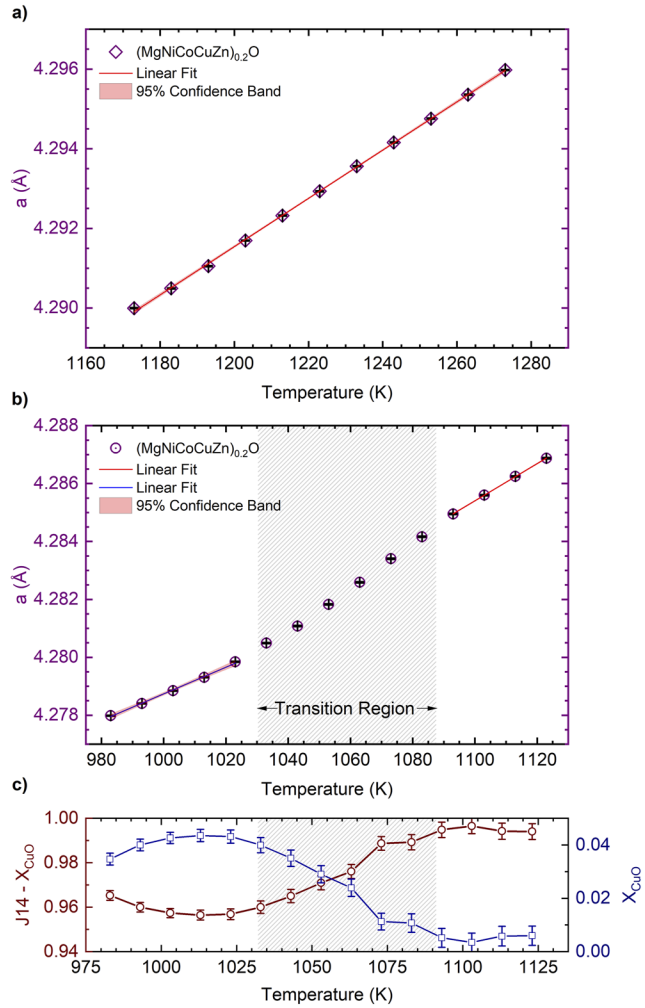

FIG. 2. Panels (a) and (b) plot the lattice parameter vs temperature below and above the multi-to-single phase transition temperature for $Mg_{0.2}Co_{0.2}Ni_{0.2}Cu_{0.2}Zn_{0.2}O$, respectively. Included with these plots are the linear fits and associated 95% confidence bands used for determining the CTE in each region of interest. Panel (c) plots the change in phase fraction across the transition temperature as determined through refinement, suggesting that ~3%–4% of CuO precipitates from J14 below the transition temperature. Between 1030 and 1090 K, CuO re-incorporates into the host matrix.

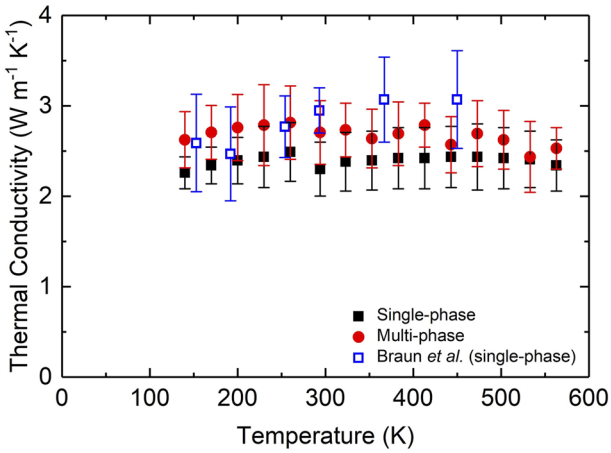

FIG. 3. The temperature dependent thermal conductivity of J14 above and below the critical temperature appears to be constant within uncertainty regardless of phase. These values agree with those reported previously, ~2.5–3 W m^{-1} K^{-1}.[31]

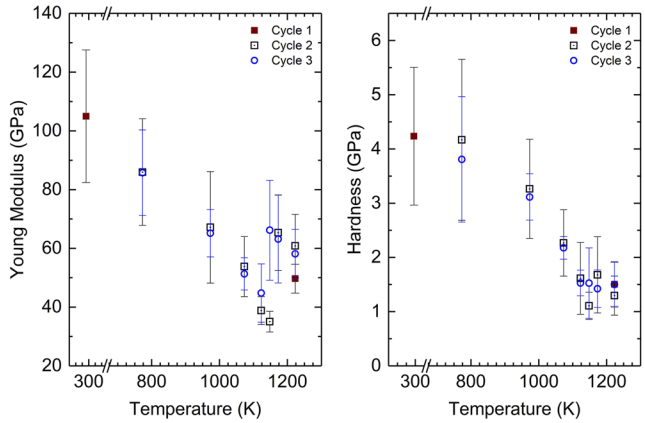

FIG. 4. Elastic modulus measurements derived from indentation. A distinctive "step" feature observed at about 1150 K, indicative of a temperature-activated stiffening mechanism. Hardness measurements derived from indentation, showing significant softening of the material above 775 K.

conductivity values were measured using the transient plane source method[30] via a hot-disk.

Within uncertainty, the thermal conductivities of the single-phase and multi-phase samples are nearly the same and span 2.5–3 W m^{-1} K^{-1}, which is in agreement with the value of 2.95 ± 0.25 W m^{-1} K^{-1} reported by Braun *et al.*[31] The primary heat carrier in both phases of J14 is phonons. The near same thermal conductivity observed here between the two phases indicates that the precipitation of CuO in the multi-phase sample does not increase phonon scattering significantly. Additionally, both phases exhibit an amorphous-like thermal conductivity trend as the temperature increases from 100 to 600 K. Such an amorphous-like trend is expected in ESOs.[31] The presence of five cations in the crystal lattice causes a significant amount of phonon scattering.[32] Furthermore, the overall porosity of the samples provides additional sites for phonon scattering.[33] Together, these two mechanisms lead to the amorphous-like thermal conductivity in single-phase and multi-phase ESOs.

As shown in Fig. 4, the specimen was observed to retain its mechanical properties through 775 K, but between 775 and 1125 K, the specimen experienced significant softening before stabilizing above 1125 K. Similarly, the elastic modulus, as shown in Fig. 4, decreased significantly within this same interval, 875–1125 K; however, there was a distinct "step" feature occurring at around 1125 K, at which point the modulus increased about 25%. This distinctive step was not present in the hardness measurement, only within the modulus measurements, indicative of a lattice-stiffening, temperature-driven mechanism. Furthermore, this step was fully detectable in both cycles 2 and 3, demonstrating the underlying mechanism to be reversible. These indentation measurements indicate the temperature-driven activation of a reversible phase transformation at about 1125 K, after which key mechanical properties may be stabilized, even slightly recovered. Hardness and modulus measurements are frequent indicators of toughening and stiffening mechanisms, respectively, and have been used in the literature to demonstrate active phase transformations in metals and ceramics.[34–36]

IV. CONCLUSIONS

The resulting effects on the thermal and mechanical properties from the reversible transformations observed in entropy-stabilized oxides were investigated. Indentation results support the previously noted phase transformation reversibility within these entropy-stabilized oxides, while temperature-dependent XRD results confirm that this mechanism is temperature-driven, not primarily stress or indentation-load driven. Importantly, the stability and even limited recovery of mechanical properties after this structure–property transformation, combined with the constant thermal conductivity, suggest that this effect may be reliably exploited for mid- to high-temperature applications of entropy-stabilized oxides. The substantial difference in the linear CTE within the regions surrounding the transition temperature may cause difficulty in applying J14 as a coating; however, to fully understand such an applied behavior, more studies would be required.

SUPPLEMENTARY MATERIAL

See the supplementary material for tables.

ACKNOWLEDGMENTS

C.M.R. and D.L.S. would like to acknowledge funding by 4-VA, a collaborative partnership for advancing the Commonwealth of Virginia. C.M.R. also acknowledges the partial support from the NSF through the Materials Research Science and Engineering Center Grant No. DMR-2011839. M.S.B.H. and P.E.H. are appreciative of the support from the Office of Naval Research, Grant No. N00014-21-1-2477. This work was performed in part at the

Analytical Instrumentation Facility (AIF) at North Carolina State University, which is supported by the State of North Carolina and the National Science Foundation (Award No. ECCS-1542015). The AIF is a member of the North Carolina Research Triangle Nanotechnology Network (RTNN), a site in the National Nanotechnology Coordinated Infrastructure (NNCI). The FIB and TEM work were performed in Colorado School of Mines Shared Instrumentation Facility Electron and Scanning Probe Microscopy Core Facility (RRID:SCR_022048).

AUTHOR DECLARATIONS

Conflict of Interest

The authors have no conflicts to disclose.

Author Contributions

Christina M. Rost: Conceptualization (equal); Data curation (equal); Formal analysis (equal); Funding acquisition (supporting); Investigation (equal); Methodology (equal); Supervision (equal); Writing – original draft (equal); Writing – review & editing (equal). **Daniel L. Schmuckler**: Formal analysis (equal); Investigation (equal); Methodology (equal); Writing – original draft (equal); Writing – review & editing (equal). **Clifton Bumgardner**: Data curation (equal); Formal analysis (equal); Methodology (equal); Writing – original draft (equal); Writing – review & editing (equal). **Md Shafkat Bin Hoque**: Data curation (equal); Formal analysis (equal); Investigation (equal); Writing – original draft (equal); Writing – review & editing (equal). **David R. Diercks**: Data curation (equal); Formal analysis (equal); Investigation (equal); Methodology (equal); Writing – original draft (equal); Writing – review & editing (equal). **John T. Gaskins**: Conceptualization (equal); Methodology (equal); Supervision (equal). **Jon-Paul Maria**: Conceptualization (equal); Resources (equal); Supervision (supporting). **Geoffrey L. Brennecka**: Conceptualization (equal); Writing – review & editing (equal). **Xiadong Li**: Supervision (equal). **Patrick E. Hopkins**: Conceptualization (equal); Funding acquisition (lead); Supervision (equal); Writing – review & editing (equal).

DATA AVAILABILITY

The data that support the findings of this study are available from the corresponding author upon reasonable request.

REFERENCES

[1] D. B. Miracle, "High-entropy alloys: A current evaluation of founding ideas and core effects and exploring "nonlinear alloys"," JOM **69**, 2130–2136 (2017).
[2] B. S. Murty, J.-W. Yeh, S. Ranganathan, and P. P. Bhattacharjee, *High-Entropy Alloys* (Elsevier, 2014).
[3] J. W. Yeh, Y. L. Chen, S. J. Lin, and S. K. Chen, "High-entropy alloys – A new era of exploitation," in *Advanced Structural Materials III, Materials Science Forum, 560* (Trans Tech Publications Ltd, 2003), pp. 1–9.
[4] R. Carroll, C. Lee, C.-W. Tsai, J.-W. Yeh, J. Antonaglia, B. A. W. Brinkman, M. LeBlanc, X. Xie, S. Chen, P. K. Liaw, and K. A. Dahmen, "Experiments and model for serration statistics in low-entropy, medium-entropy and high-entropy alloys," Sci. Rep. **5**(1), 16997 (2015).
[5] B. Cantor, I. T. H. Chang, P. Knight, and A. J. B. Vincent, "Microstructural development in equiatomic multicomponent alloys," Mater. Sci. Eng.: A **375–377**, 213–218 (2004).
[6] C. M. Rost, E. Sachet, T. Borman, A. Moballegh, E. C. Dickey, D. Hou, J. L. Jones, S. Curtarolo, and J.-P. Maria, "Entropy-stabilized oxides," Nat. Commun. **6**, 8485 (2015).
[7] T. J. Harrington, J. Gild, P. Sarker, C. Toher, C. M. Rost, O. F. Dippo, C. McElfresh, K. Kaufmann, E. Marin, L. Borowski, P. E. Hopkins, J. Luo, S. Curtarolo, D. W. Brenner, and K. S. Vecchio, "Phase stability and mechanical properties of novel high entropy transition metal carbides," Acta Mater. **166**, 271–280 (2019).
[8] J. Gild, Y. Zhang, T. Harrington, S. Jiang, T. Hu, M. C. Quinn, W. M. Mellor, N. Zhou, K. Vecchio, and J. Luo, "High-entropy metal diborides: A new class of high-entropy materials and a new type of ultrahigh temperature ceramics," Sci. Rep. **6**, 37946 (2016).
[9] S. J. McCormack and A. Navrotsky, "Thermodynamics of high entropy oxides," Acta Mater. **202**, 1–21 (2021).
[10] P. K. Davies and A. Navrotsky, "Thermodynamics of solid solution formation in NiO-MgO and NiO-ZnO," J. Solid State Chem. **38**, 264–276 (1981).
[11] J. W. Gibbs, *On the Equilibrium of Heterogeneous Substances* (American Journal of Science, 1878), p. 329.
[12] I. Levin, J. Y. Chan, J. E. Maslar, T. A. Vanderah, and S. M. Bell, "Phase transitions and microwave dielectric properties in the perovskite-like $Ca(Al_{0.5}Nb_{0.5})O_3$-$CaTiO_3$ system," J. Appl. Phys. **90**, 904–914 (2001).
[13] C. de la Calle, A. Aguadero, J. A. Alonso, and M. T. Fernández-Díaz, "Correlation between reconstructive phase transitions and transport properties from $SrCoO_{2.5}$ brownmillerite: A neutron diffraction study," Solid State Sci. **10**, 1924–1935 (2008).
[14] L. Mogni, F. Prado, C. Jiménez, and A. Caneiro, "Oxygen order–disorder phase transition in layered $GdBaCo_2O_{5+\delta}$ perovskite: Thermodynamic and transport properties," Solid State Ionics **240**, 19–28 (2013).
[15] C. Toher, C. Oses, M. Esters, D. Hicks, G. N. Kotsonis, C. M. Rost, D. W. Brenner, J.-P. Maria, and S. Curtarolo, "High-entropy ceramics: Propelling applications through disorder," MRS Bull. **47**, 194–202 (2022).
[16] A. Sarkar, L. Velasco, D. Wang, Q. Wang, G. Talasila, L. de Biasi, C. Kübel, T. Brezesinski, S. S. Bhattacharya, H. Hahn, and B. Breitung, "High entropy oxides for reversible energy storage," Nat. Commun. **9**, 3400 (2018).
[17] S. H. Albedwawi, A. AlJaberi, G. N. Haidemenopoulos, and K. Polychronopoulou, "High entropy oxides-exploring a paradigm of promising catalysts: A review," Mater. Des. **202**, 109534 (2021).
[18] B. H. Toby and R. B. Von Dreele, "*GSAS-II*: The genesis of a modern open-source all purpose crystallography software package," J. Appl. Crystallogr. **46**(2), 544–549 (2013).
[19] H. M. Rietveld, "The Rietveld method," Phys. Scr. **89**, 098002 (2014).
[20] W. C. Oliver and G. M. Pharr, "Measurement of hardness and elastic modulus by instrumented indentation: Advances in understanding and refinements to methodology," J. Mater. Res. **19**, 3–20 (2004).
[21] W. C. Oliver and G. M. Pharr, "An improved technique for determining hardness and elastic modulus using load and displacement sensing indentation experiments," J. Mater. Res. **7**, 1564–1583 (1992).
[22] M. Ridley, J. Gaskins, P. Hopkins, and E. Opila, "Tailoring thermal properties of multi-component rare earth monosilicates," Acta Mater. **195**, 698–707 (2020).
[23] Z. Ding, M. Ridley, J. Deijkers, N. Liu, M. S. B. Hoque, J. Gaskins, M. Zebarjadi, P. E. Hopkins, H. Wadley, E. Opila, and K. Esfarjani, "The thermal and mechanical properties of hafnium orthosilicate: Experiments and first-principles calculations," Materialia **12**, 100793 (2020).
[24] Y. Ho and T. K. Chu, *Electrical Resistivity and Thermal Conductivity of Nine Selected AISI Stainless Steels* (Purdue University, 1977), p. 53.
[25] M. J. Assael, S. Botsios, K. Gialou, and I. N. Metaxa, "Thermal conductivity of polymethyl methacrylate (PMMA) and borosilicate crown glass BK7," Int. J. Thermophys. **26**, 1595–1605 (2005).
[26] J. L. Braun, D. H. Olson, J. T. Gaskins, and P. E. Hopkins, "A steady-state thermoreflectance method to measure thermal conductivity," Rev. Sci. Instrum. **90**, 024905 (2019).

[27]M. Yuan, D. Bourell, and T. Diller, "Thermal conductivity measurements of polyamide 12," in *International Solid Freeform Fabrication Symposium 2011* (University of Texas Austin, 2011); available at https://repositories.lib.utexas.edu/handle/2152/88366.

[28]C.-W. Nan, R. Birringer, D. R. Clarke, and H. Gleiter, "Effective thermal conductivity of particulate composites with interfacial thermal resistance," J. Appl. Phys. **81**, 6692–6699 (1997).

[29]W. Hong, F. Chen, Q. Shen, Y.-H. Han, W. G. Fahrenholtz, and L. Zhang, "Microstructural evolution and mechanical properties of (Mg,Co,Ni,Cu,Zn)O high-entropy ceramics," J. Am. Ceram. Soc. **102**, 2228–2237 (2018).

[30]M. Gustavsson, E. Karawacki, and S. E. Gustafsson, "Thermal conductivity, thermal diffusivity, and specific heat of thin samples from transient measurements with hot disk sensors," Rev. Sci. Instrum. **65**, 3856–3859 (1994).

[31]J. L. Braun, C. M. Rost, M. Lim, A. Giri, D. H. Olson, G. N. Kotsonis, G. Stan, D. W. Brenner, J.-P. Maria, and P. E. Hopkins, "Charge-induced disorder controls the thermal conductivity of entropy-stabilized oxides," Adv. Mater. **30**, e1805004 (2018).

[32]X. Yan, L. Constantin, Y. Lu, J.-F. Silvain, M. Nastasi, and B. Cui, "$(Hf_{0.2}Zr_{0.2}Ta_{0.2}Nb_{0.2}Ti_{0.2})C$ high-entropy ceramics with low thermal conductivity," J. Am. Ceram. Soc. **101**, 4486–4491 (2018).

[33]H. Chen, H. Xiang, F.-Z. Dai, J. Liu, Y. Lei, J. Zhang, and Y. Zhou, "High porosity and low thermal conductivity high entropy $(Zr_{0.2}Hf_{0.2}Ti_{0.2}Nb_{0.2}Ta_{0.2})C$," J. Mater. Sci. Technol. **35**, 1700–1705 (2019).

[34]B. T. Wang, P. Zhang, H. Y. Liu, W. D. Li, and P. Zhang, "First-principles calculations of phase transition, elastic modulus, and superconductivity under pressure for zirconium," J. Appl. Phys. **109**, 063514 (2011); arXiv:1007.4913v1.

[35]N. Orlovskaya, K. Kleveland, T. Grande, and M.-A. Einarsrud, "Mechanical properties of $LaCoO_3$ based ceramics," J. Eur. Ceram. Soc. **20**, 51–56 (2000).

[36]B. L. Cheng, M. Gabbay, W. Duffy, and G. Fantozzi, "Mechanical loss and Young's modulus associated with phase transitions in barium titanate based ceramics," J. Mater. Sci. **31**, 4951–4955 (1996).